Surface & Coatings Technology 485 (2024) 130935

Contents lists available at ScienceDirect

Surface & Coatings Technology

journal homepage: www.elsevier.com/locate/surfcoat

Full length article

Optimisation of the laser polishing for laser-powder bed fusion and electron beam-powder bed fusion Ti6Al4V surfaces

Andrea El Hassanin [a,*], Emanuele Manco [a], Antonino Squillace [a], Muhannad Ahmed Obeidi [b,c,d]

[a] Dept. Of Chemical, Materials and Industrial Production Engineering, University of Naples "Federico II", P.le Tecchio 80, Naples 80125, Italy
[b] I-Form Advanced Manufacturing Research Centre, Dublin City University, Dublin, Ireland
[c] School of Mechanical & Manufacturing Engineering, Dublin City University, Dublin, Ireland
[d] Advanced Processing Technology Research Centre, Dublin City University, Dublin, Ireland

ARTICLE INFO

Keywords:
Powder-bed fusion
Ti6Al4V
Laser polishing
Surface quality
Microstructure

ABSTRACT

Surface quality is still one the major issues for powder-based metal additive manufacturing, affecting in a detrimental way tribology, fatigue resistance, corrosion and many other properties in comparison to their traditionally manufactured counterparts. Therefore, post-build surface finishing is required to improve surface quality. In this work, the effectiveness of laser polishing in improving the surface quality of Ti6Al4V specimens produced with Electron Beam-Powder Bed Fusion and Laser-Powder Bed Fusion was assessed. To this aim, two independent Box-Behnken designs were created to highlight the influence that the specific surface texture produced from the two additive manufacturing techniques has on the performance of laser polishing approach, also from a statistical point of view. The surface quality variations were analysed through confocal microscopy, using the areal mean roughness, Sa, as the output parameter. Microstructure and Vickers microhardness analysis were also performed to investigate the effects of laser polishing on the surface characteristics. Within the designed and investigated laser polishing windows, the results showed that laser polishing produced an appreciable surface quality improvement, of the 52 % for the case of Laser-Powder Bed Fusion and the 68 % for the case of Electron Beam-Powder Bed Fusion. Other important outcomes are related to the notable differences of the initial roughness of the L-PBF and *E*-PBF parts, affecting the performance of laser polishing: Electron Beam-Powder Bed Fusion parts had a rougher profile, with an average Sa of approximately 50 μm, if compared to Laser-Powder Bed Fusion parts for which the average Sa was approximately 10 μm in the as-built condition. This condition required a different approach for the laser polishing.

1. Introduction

1.1. Powder bed-based metal AM

Additive Manufacturing (AM), also known as 3D printing, has revolutionized the manufacturing industry by enabling the production of complex and customized parts with enhanced design freedom [1]. Additionally, the growing accessibility of several pure metals and alloys feedstocks suitable for AM contributed to the diffusion of this innovative production philosophy [2]. In this field, powder-based techniques like Laser-Powder Bed Fusion (L-PBF), Electron Beam-Powder Bed Fusion (*E*-PBF) and powder-based Directed Energy Deposition (DED) stand out as largely investigated technologies for manufacturing metal parts. These methods have gained interest due to their ability to create intricate designs and functional components using powder feedstocks. Furthermore, these technologies offer significant advantages in terms of raw material usage efficiency, parts production rate and batch dimensions, almost regardless of the part complexity. On the other hand, due to the well-known issues concerning the process dynamics such as melting track instability, balling and Marangoni effect, drawbacks such as porosity, warping, and high surface roughness are well identified problems [3]. Concerning the latter, it is known that surface roughness of metal AM parts is very high: considering the most used surface roughness indicators, namely the mean profile roughness (Ra) and the mean areal roughness (Sa), the surface roughness of as-built parts is ranging from few to tens of μm [4]. This aspect negatively affects several performances of the produced parts, such as dimensional accuracy, wear, wettability, bacterial growth, fatigue resistance to mention a few

* Corresponding author.
E-mail address: andrea.elhassanin@unina.it (A. El Hassanin).

https://doi.org/10.1016/j.surfcoat.2024.130935
Received 5 April 2024; Received in revised form 21 May 2024; Accepted 22 May 2024
Available online 23 May 2024

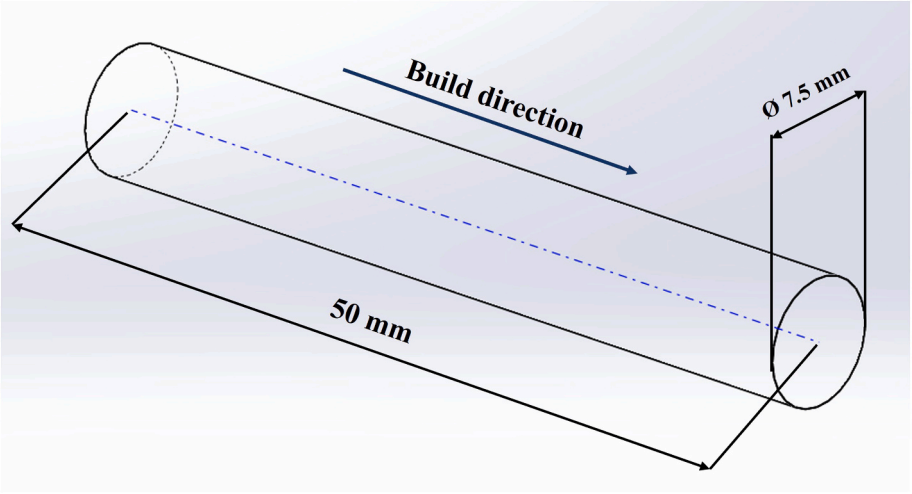

Fig. 1. Sketch of the typical specimen used for this work.

[5,6]. Among the various materials used in AM, Ti6Al4V titanium alloy is certainly one of the most employed in a wide range of sectors including aerospace, biomedical, and oil and gas extraction [5-8], due to its excellent mechanical properties. Being a $\alpha + \beta$ alloy, it is tailored to achieve specific mechanical properties through thermomechanical or thermal cycles, but preserving a satisfactory formability [9,10]. In the context of metal AM, Ti6Al4V alloy has been extensively investigated in many aspects, especially considering the case of L-PBF and E-PBF [11,12].

1.2. Surface finishing methods for powder bed-based metal AM parts

Concerning the specific aspect of the surface finishing, various techniques can be used to reduce, which can be classified based on the nature of the tool used, namely mechanical, chemical, thermal or their combination [13–17]. Mechanical treatments, such as CNC machining, shot peening, vibratory polishing, and sandblasting, rely on grinding and plastic deformation interaction mechanisms, but face limitations in accessing into many of the complex part shapes achievable with AM [18–22], even considering more unconventional technologies like Fluidized Bed Machining and Abrasive Flow Machining [23,24]. Chemical and electrochemical-based treatments offer advantages for complex parts due to the easy access of chemically aggressive solutions, especially if driven by electric potentials [14,25], but the drawbacks associated with the difficulty of finishing highly alloyed materials, process automation and control and poor sustainability are well recognised [26]. Concerning the themal-based finishing, which is mainly represented by laser polishing, many literature studies investigated the effects of laser polishing on the surface quality of metal AM parts, particularly for L-PBF processes, utilizing Nd-YAG and Yb fibre lasers. Even if it presents more limitations compared to the two previous categories of finishing methods when it comes to physical access into complex features, when laser polishing is applicable the advantages in terms of robustness and texture control are remarkable.

1.3. The current scenario of laser polishing for powder bed-based metal AM parts and aim of this work

While fibre lasers are commonly used for both L-PBF machines and ex-situ laser polishing due to their satisfactory absorption coefficient against the majority of metals and alloys [27], recent research has explored the use of pulsed lasers with ultrashort pulse durations for enhanced radiation absorption and retention of microstructure features [28,29]. In the same evolution direction, still not focused on the surface polishing aspect yet still applicable, the use of laser with reduced wavelength, known as green laser and blue laser, demonstrated to be quite promising for the processing of highly reflective materials including copper in the case of L-PBF, *E*-PBF and powder-based DED leading to excellent densification and microstructure with lower energy input required in comparison with fibre laser [30,31]. On the other hand, recent studies also reported that long wavelength laser sources, such as CO_2-based ones, can be effectively used despite their lesser

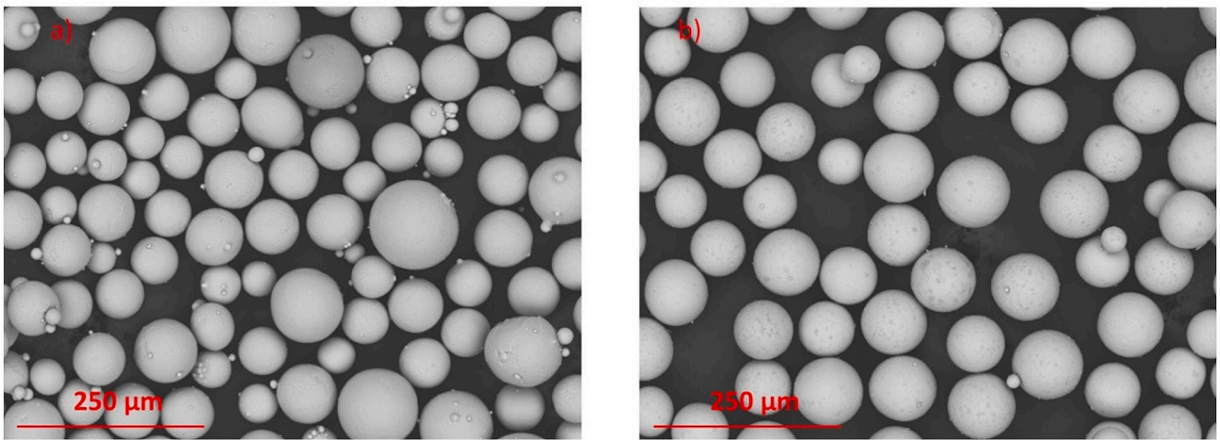

Fig. 2. SEM images of the powder feedstocks used for: a) Arcam Ti6Al4V powders for *E*-PBF and b) Renishaw Ti6Al4V powders for L-PBF.

Table 1
Chemical composition of the powder feedstocks.

AM process	Element	Ti	Al	V	Fe	O	C	N	H
L-PBF	wt%	bal.	5.5–6.5	3.5–4.5	<0.25	<0.13	<0.08	<0.03	<0.013
E-PBF		bal.	5.5–6.8	3.5–4.5	<0.30	<0.20	<0.10	<0.05	<0.015

absorption efficiency by taking advantage of the rough surfaces in the as-built condition [32]. Considering the overall scenario, the wide literature data available concerning the laser polishing development witnesses the relevancy of the topic for metal AM parts, but little or no data are available concerning the influence that the different roughness levels produced from the L-PBF and *E*-PBF processes has on the development route of laser polishing. Based on this premise, this work proposes an experimental optimisation analysis of the influence of CO_2 laser polishing on both *E*-PBF and L-PBF Ti6Al4V parts, exploiting the main processing aspects and issues when considering parts coming from the same family of manufacturing techniques but with significant differences in terms of surface quality. In other terms, this work tries to fill to the following knowledge gap: i) if the surface morphologies of L-PBF and *E*-PBF parts are different, there is a need for different laser polishing parameters? ii) if so, given that E-PBF produced surfaces are more rough, a better result is expected due to enhances laser absorption? iii) what are the effects on surface chemistry, microstructure and hardness?

2. Materials and methods

2.1. Ti6Al4V AM specimens

In this study, Ti6Al4V alloy cylindrical specimens were produced through *E*-PBF and L-PBF, built vertically with respect to the build platform. Fig. 1 shows the design of the specimen with the related dimensions. Fig. 2 shows the SEM images of the respective powders used for the fabrication, whose chemical composition is also reported in Table 1. The powder size distributions, measured according to the ASTM B822 standard, were the following: D_{10} = 21 μm; D_{50} = 37.3 μm; D_{90} = 54 μm for the L-PBF process (SLM solutions GmbH) — D_{10} = 52 μm; D_{50} = 71 μm; D_{90} = 102 μm for the *E*-PBF process (Advanced Powders – General Electric). It is worth to mention that the difference in size between the two feedstocks is dictated by the different processing ability of the electron beam against the laser: the former is generally larger in spot and with higher power, leading to the capacity of processing larger layer thicknesses and hence being more productive in comparison with the laser [33]. However, at the same time, this difference leads in poorer surface quality of *E*-PBF parts compared to L-PBF parts. The L-PBF specimens were produced by means of a Renishaw AM250 L-PBF machine, with the following process parameters: laser power = 350 W, hatch distance = 55 μm, layer thickness = 30 μm; contour strategy: disabled. The printing process was carried out in Argon atmosphere. The build platform was preheated to 400 °C in order to minimize distortion and for a better control over cooling rates, and the scanning strategy was raster type with a rotation of 67° between two consecutive layers. For the *E*-PBF specimens, an Arcam A2X E-PBF machine was used. The specimens were produced according to the following parameters: gun voltage = 60 kV, hatch distance = 55 μm, layer thickness = 90 μm. The build platform was maintained at a temperature of 730 °C, and the beam scanning, carried out according to the integrated speed function supplied by Arcam for the selected alloy, was raster-like as similarly to the L-PBF process. The entire printing process was carried out under vacuum 1.6×10^{-4} mBar before starting the high voltage supply.

2.2. Laser polishing

The laser polishing process was performed using a ROFIN DC-15 1.5 kW CO_2 laser, with the following characteristics: maximum power = 1.5 kW; source wavelength = 10.64 μm; beam quality factor (M^2) = 1.05; laser focus = 200 μm; working mode: continuous wave; assist gas: Argon. The test specimens were connected to the variable speed DC motor by means of a holding chuck in order to facilitate the rotational movement (maximum speed = 5000 rpm), as shown in Fig. 3a. This assembly was mounted onto the positioning stage of the CO_2 laser, as shown in Fig. 3b. The CNC control system was utilized to control the translational movement of the stage (maximum speed = 5000 mm/min), enabling linear displacement of the sample with reference to the fixed laser beam as shown in Fig. 3a. By combining both linear and rotational motions, a series of overlapping laser scanning tracks (OV) were generated, effectively covering the targeted surface area during the scanning process [10].

Following an approach based on a previous study conducted by Obeidi et al. [10] and after performing few preliminary tests, the influence of several processing parameters was investigated based on a Design of Experiment DoE model. More specifically, a Box-Benkhen Design (BBD) with three factors in three levels was considered, with the aim to reduce the number of experiments in comparison with a full factorial design. The factors considered were the laser power, the percentage overlap between the laser tracks (OV%) and number of passes. The chosen polishing parameters used for *E*-PBF and L-PBF specimens

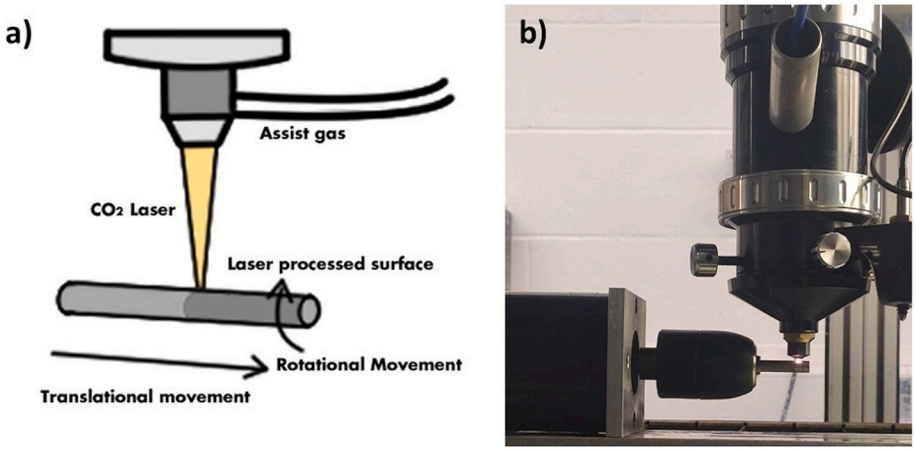

Fig. 3. a) Sketch of the laser polishing setup; b) Actual experimental setup.

Table 2
Factors and levels considered for the BBD of laser polishing of E-PBF and L-PBF specimens.

E-PBF	Power (W)	OV (%)	Number of Passes	Translational speed (mm/min)	Rotational speed (RPM)
Level 1	135	0	2		300
Level 2	150	33	3	60	450
Level 3	165	50	4		600
L-PBF	Power (W)	OV (%)	Number of Passes	Translational speed (mm/min)	Rotational speed (RPM)
Level 1	135	0	1	20	
Level 2	150	25	2	30	200
Level 3	165	50	3	40	

respectively are reported in Table 2. Consequently, considering five repetitions of the centerpoint, a total of 17 polishing experiments were carried out for each specimen type, as reported in Tables 3 and 6 for the E-PBF and L-PBF processes respectively. For any other experimental condition apart from the centerpoints, three repetitions were considered. All the laser polishing experiments were carried out with a laser spot of 200 μm and using Argon shielding gas at a pressure of 0.3 bar. Considering the OV%, it can be controlled by either varying the translational speed or the rotational speed: based on a first process development documented elsewhere [10], for the L-PBF case the control of the OV% was carried out by varying the translational speed. The results from the L-PBF BBD were used as starting point for the *E*-PBF BBD: using the best parameters combination from the L-PBF BBD on E-PBF samples, it was noted that the selected parameters were not significantly affecting the surface as expected, given the higher roughness. For this reason, more consecutive passes without idle times (2 to 4, rather than 1 to 3) were required to polish E-PBF specimens but, to avoid overmelting, the rotational speed was set to higher levels than the L-PBF case, thus it was selected as the controlling parameter for OV%. In any case, considering the geometry of the specimen illustrated in Fig. 1, each laser polishing experiment produced a polished area with a width of 5 mm along the specimen's axis. Moreover, for the case of multiple passes, no idle time was considered between each pass.

2.3. Surface quality, morphology, and microstructure characterization

The surfaces of both the as-built and laser-polished specimens were characterised by using a Bruker Contour GT 3D optical microscope. The instrument was equipped with the VISION 64® software for data analysis, surface profile visualization, and surface roughness description term evaluation. For the surface acquisitions, a 1 × 1.2 mm area was investigated. Concerning the measured outputs, it was decided to analyse Sa, already mentioned in the introduction section and defined according to the ISO 25178 standard. Moreover, given the adoption of a DoE approach for the experiments, it was decided to analyse the effects of the treatment and its input variables on the surface quality through the Response Surface Method (RSM). In this way, assuming a 95 %

Table 3
BBD considered for the E-PBF specimens and Sa post-polishing (mean ± st.dev).

Power (W)	Passes	OV (%)	RPM	Translational speed (mm/min)	Single pass polishing time (s)	Total polishing time (s)	Sa (μm)
150	3	33	450	60	5	15	17,9 ± 2.2
135	2	33	450	60	5	10	14,7 ± 2.8
150	3	33	450	60	5	15	18,7 ± 2.5
135	3	0	300	60	5	15	15,2 ± 2.4
150	3	33	450	60	5	15	17,4 ± 1.5
150	4	50	600	60	5	20	18,1 ± 3
150	3	33	450	60	5	15	21,2 ± 3.1
150	3	33	450	60	5	15	18,2 ± 1.3
165	3	50	600	60	5	15	12,7 ± 1.1
135	3	50	600	60	5	15	20,2 ± 2.8
150	2	0	300	60	5	10	21,9 ± 1.5
165	3	0	300	60	5	15	11,1 ± 2.1
150	4	0	300	60	5	20	12,1 ± 1
135	4	33	450	60	5	20	18,1 ± 2.5
165	4	33	450	60	5	20	16,6 ± 1
165	2	33	450	60	5	10	15,8 ± 3.7
150	2	50	600	60	5	10	24,8 ± 2

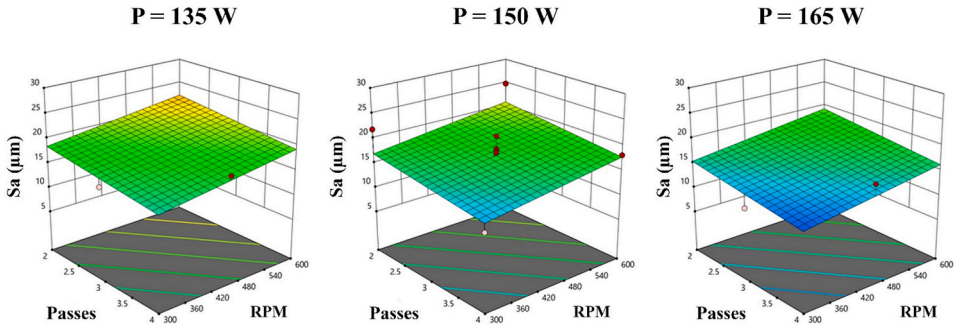

Fig. 4. Response surfaces obtained for the *E*-PBF specimens after laser polishing. The plots show the correlation between Sa and passes-rpm, for each level of laser power. The red points indicate experimental values greater than the predicted, vice versa for the white ones.

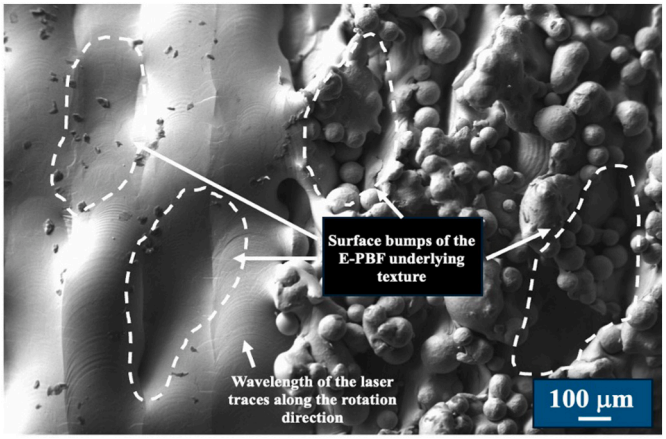

Fig. 5. SEM image taken at the interface between the as-E-PBF and laser polished surfaces, showing the significant improvement of the surface quality. The picture shows the best results obtained from the Box Behnken of E-PBF.

confidence interval (i.e. $\alpha = 0.05$), the correlation between the input and output variable was analysed also from a statistical point of view through a multivariate ANOVA. Afterwards, the surface morphology inspection before and after the laser polishing was analysed through SEM-EDS (Hitachi TM3000 SEM – Oxford Instruments SWIFTED3000 EDS probe). After a metallographic preparation, SEM-EDS analyses were also carried out on cross-sections for microstructural evaluations, of in combination with optical microscopy (Zeiss Axioskop 40). The cross-sections were prepared through cutting, hot mounting and polishing until 1 µm, followed by etching with Keller's reagent by swabbing for 20 s. Finally, Vickers microhardness measurements were performed on the cross sections (CV Instruments 2000), performing at least three indentations on the polished area and bulk material, with a 500 g load and 15 dwell time.

3. Results and discussion

3.1. Laser surface polishing of E-PBF specimens

For the case of the E-PBF specimens, it was found that Sa of the as-built specimens was 54.3 ± 4.1 µm, presenting therefore a quite rougher surface compared to the case of L-PBF. This result was expected considering the nature of the *E*-PBF process, involving powders with larger size in the first place in comparison with L-PBF as well as a more intense thermal interaction due to the electron beam in substitution of the laser [34]. For what concerns the effects of laser polishing, Fig. 4 shows the response surfaces, sorted by the laser power levels and showing the effects of the other variables on Sa.

Table 4
Model fitting summary for the laser polishing BBD of E-PBF specimens.

	Sum of Squares	Degrees of freedom	Mean Square	F-value	p-value
Model (linear)	67.03	3	22.34	2.10	0.1493
No. of passes (A)	18.94	1	18.94	1.78	0.2047
RPM (B)	29.88	1	29.88	2.81	0.1174
Laser power (C)	18.21	1	18.21	1.71	0.2131

As visible from the 3D plots, the effects of the investigated process variables can be fitted with a linear regression, given the appreciable but not steep differences in Sa among the BBD combinations. In general, the main experimental outcome was that the laser polishing had a significant effect on the surface quality of *E*-PBF specimens, with an average final value of about 17.3 ± 3.3 µm, indicating therefore an average Sa reduction of the 68 % of the starting values. This appreciable reduction of roughness can be seen also from the SEM image reported in Fig. 5 that shows that the huge amount of sintered powders on the surface due to the E-PBF process were completely removed after polishing but, at the same time, preserving the wavy mark of the underlying E-PBF surface morphology caused by the molten track instability during the print. This effect of polishing was supported by the notable difference in wavelength between the laser shifts along the circumferential direction and the surface bumps which are residuals of the original *E*-PBF texture that underlies the layer of sintered powders, as also proved by the similar size of the bumps observed in both the polished and as-built areas according to the dashed areas illustrated in Fig. 5.

However, despite the appreciable improvement of the surface quality, the investigated processing window did not allow to exploit significant correlations between the inputs and Sa. More specifically, despite the requirements of normality and randomness of the variance were satisfied, as visible in Fig. 6, the ANOVA results showed that the levels

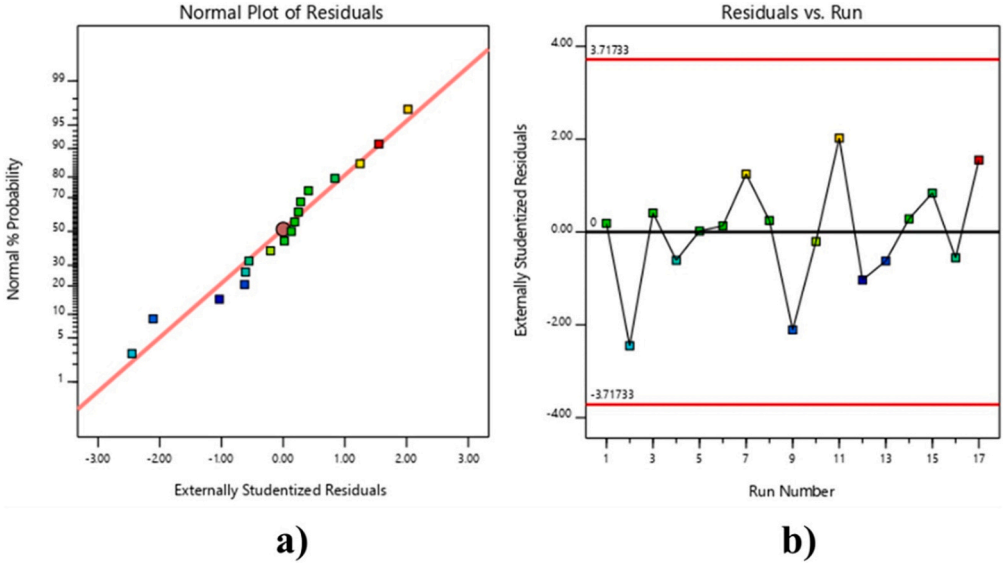

Fig. 6. a) Normal probability plot of the post-laser polishing residuals, showing that the results meet the requirement of data normality for the subsequent regression; b) Analysis of variance vs run number, showing the absence of specific trends that suggests the absence of systematic experimental errors.

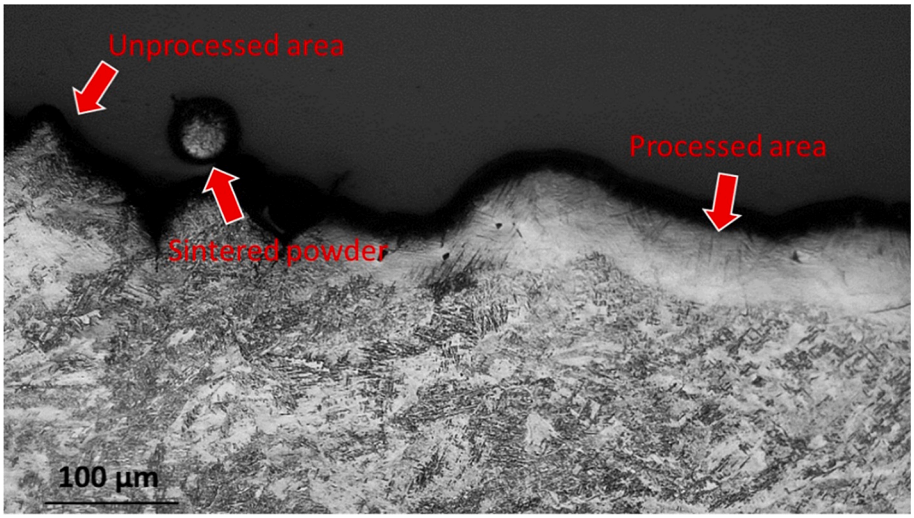

Fig. 7. Optical macrograph of a laser-polished *E*-PBF specimen, taken at the interface between the as-built and polished areas (magnification 100×).

chosen for the factors were not providing a statistical significance, as noticeable from the ANOVA summary data reported in Table 4. In other terms, the influence of the operating parameters on the surface modification entity was not sufficiently different among the processing combinations to draw robust conclusions. Indeed, the regression analysis led to a signal-to-noise ratio of 4.39, hence slightly sufficient to proceed with the regression according to the Design Expert software indications, and an adjusted R^2 of 0.17, that suggests an overall weak correlation between the model terms, i.e. the input variables, and Sa. This outcome can be also seen according to the *p*-value results reported in Table 7, showing that in every case it was greater than fixed confidence value of 0.05.

The poor statistical robustness of the model could be interpretated according to the analysis of the phenomena behind the observed experimental outcomes. The experimental results proved the feasibility of the laser polishing process in reducing the surface roughness of E-PBF specimens, however, Fig. 5 showed clearly that the greatest contribution of this reduction was due to the melting of the sintered powders, leaving a jagged and wavy surface. The latter residual texture characteristic could be ascribed to two main factors: i) the high initial surface roughness: as the laser ability to re-melt the superficial material depends from the energy input in the first place, there is evidence in literature that the laser polishing of rough surfaces such as the ones typical of powder-based AM could benefit of an enhanced absorption due to multiple rebounding of the beam into the asperities [35,36]. On the other hand, when the initial surface roughness is very high such as in this case, this benefit could be limited and might lead also to a relatively lower surface quality compared to the L-PBF specimens. Achieving high surface quality (low Sa) is correlated to more exposure to the laser beam, more melting and may include some material removal through ablation. This statement is also supported by the response surfaces reported in Fig. 4 showing that longer laser residence times, achieved mainly by increasing the number of consecutive passes which reflects on the total polishing time (see Table 3), leads to lower Sa. Therefore, the presence of superficial bumps on the polished surface might be due to the residues of the original topography lying underneath the sintered powders layer; ii) the focal position of the laser on the specimen surface: in this work, the laser spot was set as equal to its focus, placed at the same height of the surface peaks. Consequently, taken again into account the irregularity and asperities height variation of the as-built surface, a small beam diameter with a close focal position could affect detrimentally the robustness of the re-melting mechanism against these height differences. Hence, the possibility to better discriminate the efficiency of different combinations of power, speed and OV% becomes more difficult, leading to the closeness of the results shown in Fig. 4. As a matter of fact, the benefits on the surface quality improvement deriving from the laser defocusing was already discussed elsewhere [36]. Further evidence that supports this point can be found from the optical macrograph illustrated in Fig. 7, showing a cross section of the interface as-built-polished surface from the best-case specimen (lowest Sa), taken along the specimen axis. As the asperities observed in the as-built surface appear very high, it is convincible that the laser was not able to transfer energy for re-melting in a balanced way against the different peaks and valleys, introducing conversely also a waviness component on the polished surface due to the insufficient re-melting energy. Furthermore, Fig. 7 highlights, as expected, also the presence a re-molten superficial layer,

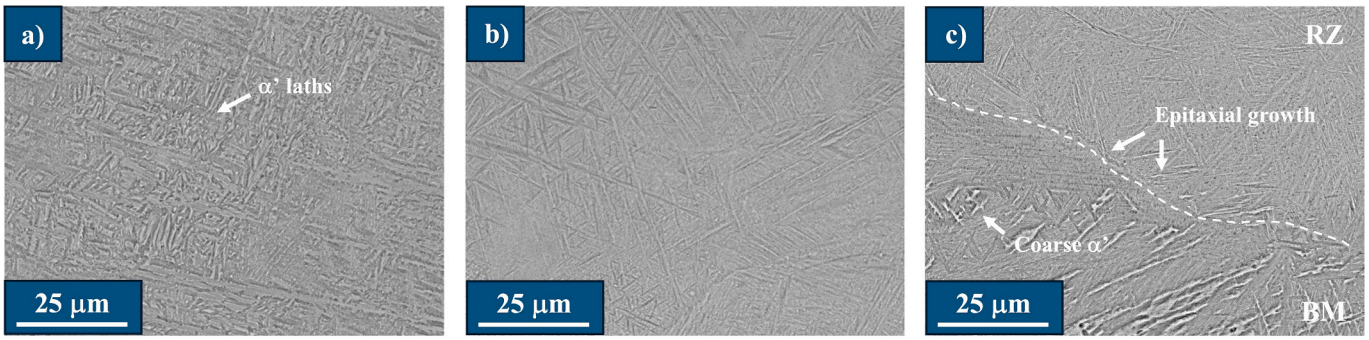

Fig. 8. SEM micrographs illustrating the microstructure of the: a) Base material (BM); b) *Re*-molten zone (RZ); c) interface between BM and RZ (magnification 2000×).

Table 5
Chemical composition data of the base material and re-molten zone, obtained through EDS analysis (mean ± st.dev).

Element (wt%)	Ti	Al	V
Base material	90.8 ± 0.1	5.1 ± 0.1	4.0 ± 0.1
Re-molten zone	90.2 ± 0.1	5.8 ± 0.1	4.0 ± 0.1

whose depth was around 50 μm and their microstructure features were quite comparable to the ones of the parent alloy, as shown from the SEM-EDS results illustrated in Fig. 8 and Table 5 respectively. Overall, the microstructure variation induced by polishing consisted in a transition from a martensitic microstructure (α' phase, Fig. 8a) of the base material to a fine lamellar and basket-weave crystal structure of the re-molten layer (Fig. 8b), which would suggest that the cooling rate of the alloy during polishing was lower compared to the case of *E*-PBF, starting in both case from the molten state of the material and, hence, at a temperature above the beta transus [37]. Moreover, as shown in Fig. 8c, it seems that in the interface region between the two zones, a slight coarsening of the lamellar martensite occurred and the epitaxial growth of the fine α + β lamellae, both which are often encountered mechanisms in AM of the Ti6Al4V alloy [38]. Nevertheless, all the microstructure changes found were not accompanied by any significant variation in Vickers microhardness: for the parent material, the microhardness was 325 ± 25 HV, whereas for the polished zone was 351 ± 15 HV.

3.2. Laser surface polishing of L-PBF specimens

For the case of the L-PBF specimens, it was found that Sa of the as-built specimens was 10.2 ± 1.1 μm, showing therefore a smoother surface texture compared to E-PBF. However, despite this expected outcome, the response surfaces illustrated in Fig. 9 highlight that the influence of the polishing variables on Sa was more evident in comparison to the *E*-PBF case, as also confirmed by the data reported in Table 6. More specifically, it can be noted that: i) the response surface indicated as optimal a number of passes of 2; ii) for the conditions related to a high-residence time of laser on the surface (low translation speed, high number of passes), an increase of the laser power had a negative effect on the polishing efficiency.

Overall, the laser polishing produced a Sa reduction of the L-PBF specimens of about the 52 %, with a final value of 5.4 ± 0.5 μm. Once again, the quantitative results were supported by the SEM inspection of the surface, indicating a remarkable surface modification occurred through the removal of sintered powder formed by balling. Moreover, it is also interesting to observe that the underlying morphology was flatter than the *E*-PBF typical one, giving therefore evidence that the different as-built surface has a great influence on the polishing efficiency (Fig. 10).

As visible from the curvature of the response surfaces reported in Fig. 9, a higher-order fitting model (quadratic) was found to be the best for the L-PBF polishing case. As for the E-PBF case, the normality of the residues as well as the randomness of the variance vs experiments ID was checked through Design Expert ®, whose results are reported in Fig. 11.

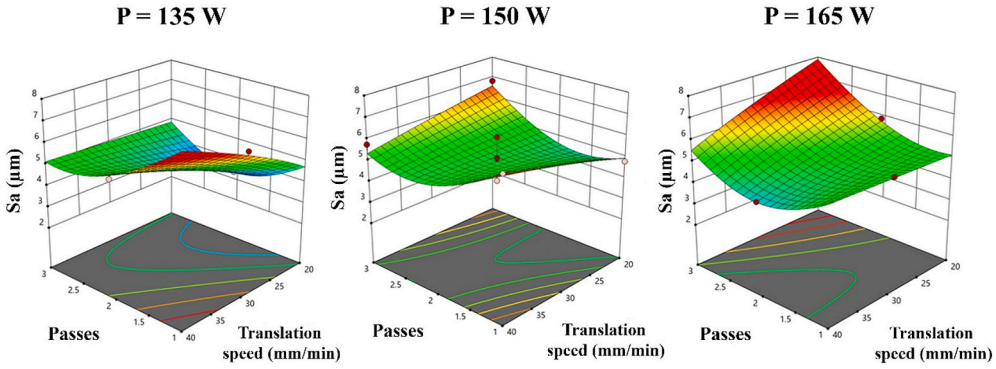

Fig. 9. Response surfaces obtained for the L-PBF specimens after laser polishing. The plots show the correlation between Sa and passes-translation speed, for each level of laser power. The red points indicate experimental values greater than the predicted, vice versa for the white ones.

Table 6
BBD considered for the L-PBF specimens and Sa post-polishing (mean ± st.dev).

Power (W)	Passes	OV (%)	RPM	Translational speed (mm/min)	Single pass polishing time (s)	Total polishing time (s)	Sa (μm)
150	3	50	200	20	15	45	6,8 ± 1.3
150	2	25	200	30	10	20	5,1 ± 0.1
150	1	50	200	20	15	15	4,8 ± 1
150	1	0	200	40	7.5	7.5	6,7 ± 0.2
135	3	25	200	30	10	30	4,8 ± 1.8
135	2	50	200	20	15	30	3,4 ± 0.1
150	2	25	200	30	10	20	4,9 ± 1.1
165	1	25	200	30	10	10	5,4 ± 1.1
165	3	25	200	30	10	30	6,5 ± 1.8
150	2	25	200	30	10	20	6,0 ± 1.9
135	1	25	200	30	10	10	6,6 ± 1.1
165	2	0	200	40	7.5	15	4,4 ± 0.4
135	2	0	200	40	7.5	15	5,5 ± 0.3
150	3	0	200	40	7.5	22.5	5,8 ± 1.3
150	2	25	200	30	10	20	4,0 ± 1
165	2	50	200	20	15	30	5,9 ± 1.3
150	2	25	200	30	10	20	4,6 ± 0.2

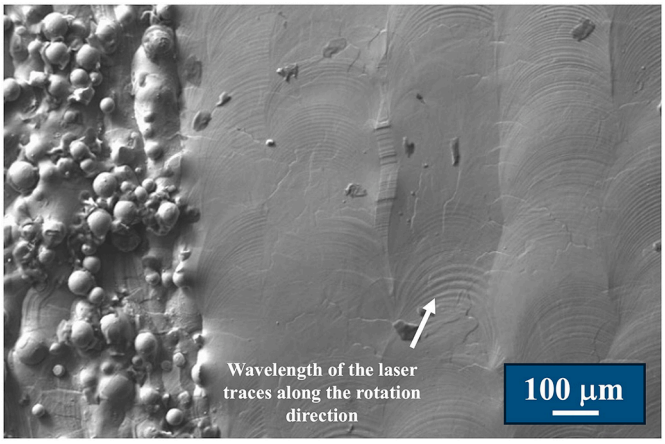

Fig. 10. SEM image taken at the interface between the as-L-PBF and laser polished surfaces, showing the significant improvement of the surface quality. The picture shows the best results obtained from the Box Benkhen of L-PBF.

The results indicated again that the experimental data were suitable for the surface regression. Concerning the latter, Table 7 shows the fitting model summary and the terms chosen for the model. Besides the factors chosen for the polishing experiments, the model included also coupled-interfering factors and a time-autocorrelation factor related to the number of passes. It is worth to mention that the same quadratic terms for the translation speed and power were removed from the model, as they were constant for each experiment and therefore not meaningful for the regression. Overall, the regression analysis led to a signal-to-noise ratio of 8.64 and an adjusted R^2 of 0.7, suggesting therefore a stronger correlation between the input variables and Sa. However, according to the *p*-values reported in Table 7, it can be seen that the statistically significant terms were the interaction factors, except for the one that couples the laser power (C) and the translational speed (B), and the quadratic term for the number of passes. This result could be justified according to the following considerations: i) as the laser polishing relies on the heat input provided by the laser, whose way of adduction is regulated through the scanning factors (in this case, translational the speed and the number of passes), it is convincible that the overall process dynamics is dictated by the combination of the provided energy input and the residence time of the laser over a defined area, hence providing more physical sense of grouped variables against the individual ones. However, the latter were still kept in the model as they were chosen as the actual inputs; ii) the re-melting ability of the laser depends strongly on the number of consecutive passes, either from a surface status and thermal history points of view. For the former aspect, even if the surface is smoothed after the first laser pass, the processed material is still able to absorb the radiation and experience re-melting, as also proven in more challenging cases like the aluminum [4]. Furhermore, the benefits of the multiple consecutive passes could benefit from the heat build-up effect experienced from the specimen as it helps to stabilize the melting pool by reducing local temperature gradients; iii) as the ratio between the laser power and the translational speed determines the energy input for a single laser track [4], the BC interaction factor falls into a multi-collinearity with the individual ones, causing then the loss of statistical significance in the model.

Concerning the influence of the as-built surface morphology of the specimens on the effectiveness of laser polishing, a variable onto which a particular attention was given in this work by selecting 2 AM processes, a support to all the observed experimental and statistical outcomes can be found by looking the optical macrograph reported in Fig. 12. Comparing the two best cases from the two different technologies, the macrograph shows that surface morphology of the as-L-PBF condition is more stable compared to the *E*-PBF case, in terms of the waviness underlying the sintered powders layer. Consequently, the laser re-melting sensitivity against the surface height differences is reduced, being still valid the enhanced radiation absorption mechanism through the rough

Table 7
Model fitting summary for the laser polishing BBD of L-PBF specimens.

	Sum of Squares	Degrees of freedom	Mean Square	F-value	p-value
Model (quadratic)	1484.5	7	212.1	6.26	0.0069
No. of passes (A)	2.34	1	2.35	0.0691	0.7985
Translation speed (B)	17.12	1	17.12	0.5058	0.4950
Laser power (C)	33.34	1	33.34	0.9848	0.3469
AB interaction	302.75	1	302.75	8.94	0.0152
AC interaction	290.16	1	290.16	8.57	0.0168
BC interaction	291.39	1	291.39	8.61	0.167
A time-autocorrelation (A^2)	547.44	1	547.44	16.17	0.0030

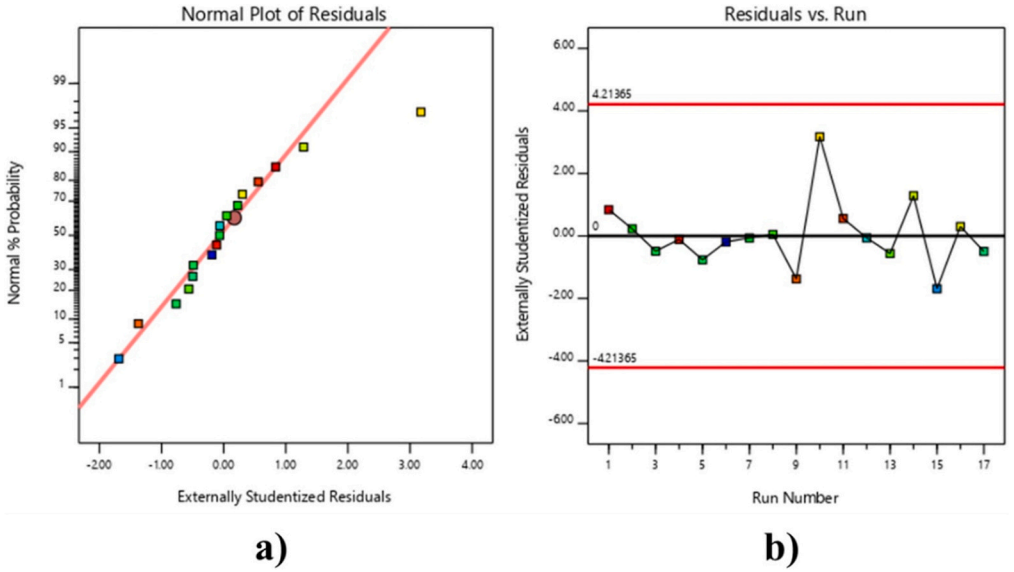

Fig. 11. a) Normal probability plot of the post-laser polishing residuals, showing that the results meet the requirement of data normality for the subsequent regression; b) Analysis of variance vs run number, showing the absence of specific trends that suggests the absence of systematic experimental errors.

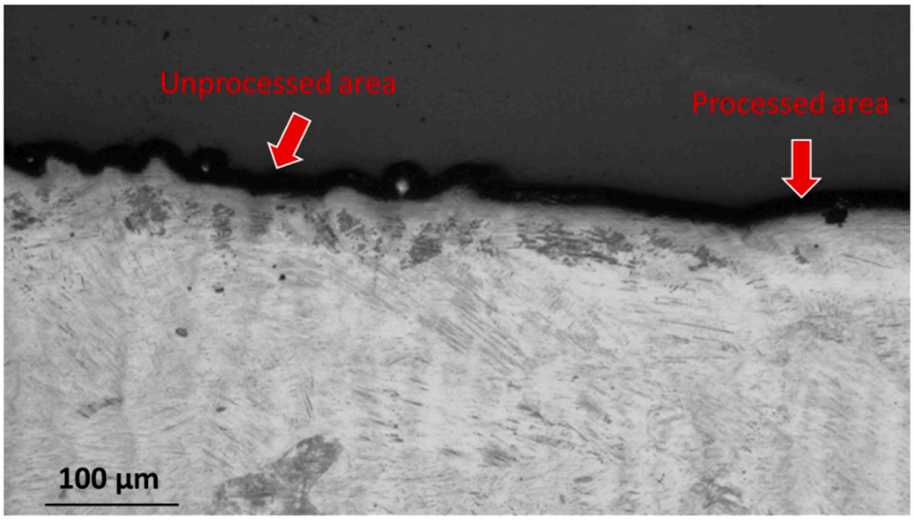

Fig. 12. Optical macrograph of a laser-polished L-PBF specimen, taken at the interface between the as-built and polished areas (magnification 100×).

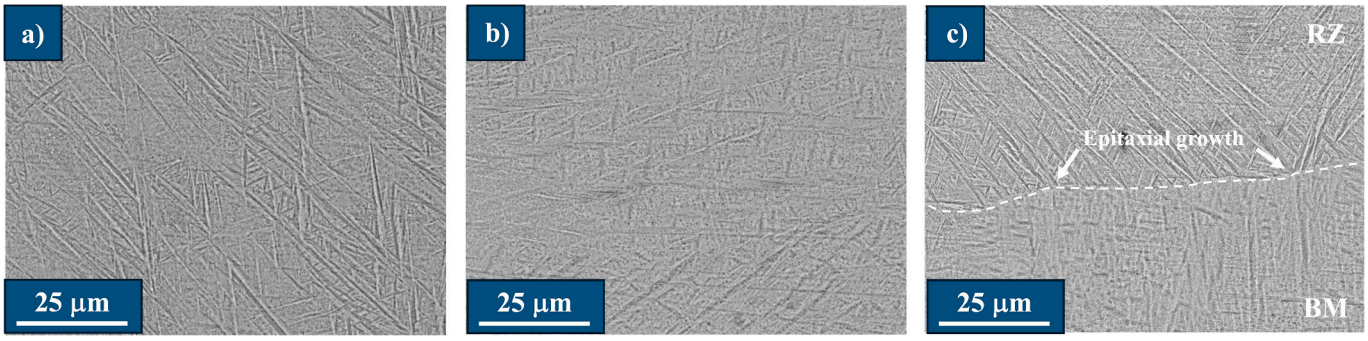

Fig. 13. SEM micrographs illustrating the microstructure of the: a) Base material (BM); b) *Re*-molten zone (RZ); c) interface between BM and RZ (magnification 2000×).

Table 8
Chemical composition data of the base material and re-molten zone, obtained through EDS analysis (mean ± st.dev).

Element (wt%)	Ti	Al	V
Base material	90.0 ± 0.2	5.9 ± 0.1	4.1 ± 0.2
Re-molten zone	90.3 ± 0.2	6.0 ± 0.1	3.7 ± 0.2

initial surface, especially for the first laser pass. In any case, it is still expected that an upward defocusing of the laser beam could contribute to a further improvement of polishing and increase the roughness reduction. For what concerns the microstructure evolution of the laser-processed surface, similar consideration of the E-PBF case can be drawn, as the re-molten layer depth was again around 50 µm, as visible in Fig. 12, and no significant microstructural nor chemical composition alterations occurred according to the results reported in Fig. 13 and Table 8 respectively. The only exception in this case was that the crystal structure of the base material and of the re-molten layer was always basket-weave type. Consequently, also the Vickers microhardness was not particularly affected the polishing process: in this case, the micro-hardness of the base material was 378 ± 32 HV, whereas for the polished zone was 384 ± 30 HV.

4. Conclusions

This work was focused on the optimisation of the laser surface polishing of Ti6Al4V alloy specimens manufactured via *E*-PBF and L-PBF technologies. For both the cases, polishing experiments were carried out according to ad-hoc Box-Behnken Designs that considered the great surface morphology differences between the 2 AM techniques as well as the main polishing governing factors. According to the obtained results and the related discussion, the following conclusions can be drawn:

- The laser polishing provided a more appreciable roughness reduction, analysed through S_a, for the *E*-PBF case (68 % for the best case) in comparison to the L-PBF one (52 % for the best case). According to the quite higher initial roughness of the as-built E-PBF specimens (54.3 ± 4.1 µm) against the L-PBF ones (10.2 ± 1.1 µm), this result was somehow expected considering the enhancing of the laser absorption when increasing the roughness of the surface under polishing, as well as the different polishing conditions investigated considering the need for more laser passes in the case of *E*-PBF (from 2 to 4) in comparison to L-PBF (from 1 to 3).
- On the other hand, the very irregular surface morphology that implied the benefit highlighted in the previous point was also one of the major responsible for the weak correlation between the polishing parameters (specimen rotational speed, laser power, number of passes) and the roughness reduction for the E-PBF case, as proved by an adjusted R^2 of the linear model of 0.17. This result was mainly ascribed to the high sensitivity of the re-melting ability of the laser against the surface unevenness.
- Based on the previous point, a different conclusion was drawn for the case of polishing of L-PBF specimens, for which a quadratic model was found to be the best fit to the experimental data that provided an adjusted R^2 of 0.7. More specifically, the very statistically significant

terms of the model were the coupled-interfering ones and the time-autocorrelation factor related to the number of passes.

- The microstructure alterations after polishing were remarkable only in the E-PBF case, consisting in a transition from a martensitic microstructure to a fine and basket-weave one. However, both the chemical composition and Vickers microhardness were not significantly affected after polishing.
- As a future remark, the experimental outcomes obtained in this work would be useful as a basis to investigate the different response of the laser-processed surfaces coming from different metal AM technologies on fatigue, corrosion, wear, wettability and other properties.

CRediT authorship contribution statement

Andrea El Hassanin: Writing – review & editing, Writing – original draft, Methodology, Investigation, Formal analysis, Data curation. **Emanuele Manco:** Writing – original draft, Validation, Methodology, Investigation, Formal analysis, Data curation. **Antonino Squillace:** Supervision, Project administration, Funding acquisition, Data curation. **Muhannad Ahmed Obeidi:** Writing – review & editing, Project administration, Methodology, Investigation, Funding acquisition, Formal analysis, Data curation.

Declaration of competing interest

The authors declare that they have no known competing financial interests or personal relationships that could have appeared to influence the work reported in this paper.

Data availability

Data will be made available on request.

Acknowledgments

This research is supported in part by a research grant from the Science Foundation Ireland (SFI) under grant number 16/RC/3872 and 18/EPSRC-CDT/3584 and is co-funded under the European Regional Development Fund and by I-Form Industry partners. The authors acknowledge the financial support from the Faculty of Engineering and Computing, Dublin City University.

References

[1] I. Gibson, D. Rosen, B. Stucker, M. Khorasani, Industrial Drivers for AM Adoption, 2021, https://doi.org/10.1007/978-3-030-56127-7_21.
[2] W.E. Frazier, Metal additive manufacturing: a review, J. Mater. Eng. Perform. 23 (2014) 1917–1928, https://doi.org/10.1007/s11665-014-0958-z.
[3] T. DebRoy, H.L. Wei, J.S. Zuback, T. Mukherjee, J.W. Elmer, J.O. Milewski, A. M. Beese, A. Wilson-Heid, A. De, W. Zhang, Additive manufacturing of metallic components – process, structure and properties, Prog. Mater. Sci. 92 (2018) 112–224, https://doi.org/10.1016/j.pmatsci.2017.10.001.
[4] A. El Hassanin, M.A. Obeidi, F. Scherillo, D. Brabazon, CO2 laser polishing of laser-powder bed fusion produced AlSi10Mg parts, Surf. Coat. Technol. 419 (2021), https://doi.org/10.1016/j.surfcoat.2021.127291.
[5] E. Manco, F. Scherillo, A. El Hassanin, D. Borrelli, A. Caraviello, A. Squillace, Experimental setup for fatigue testing of additively manufactured specimens, Key Eng. Mater. 926 KEM (2022) 141–146, https://doi.org/10.4028/p-mgf52c.
[6] A. Krishnan, F. Fang, Review on mechanism and process of surface polishing using lasers, Front. Mech. Eng. 14 (2019) 299–319, https://doi.org/10.1007/s11465-019-0535-0.
[7] J.A. Tamayo, M. Riascos, C.A. Vargas, L.M. Baena, Additive manufacturing of Ti6Al4V alloy via electron beam melting for the development of implants for the biomedical industry, Heliyon 7 (2021) e06892, https://doi.org/10.1016/j.heliyon.2021.e06892.
[8] H. Nguyen, A. Pramanik, A.K. Basak, Y. Dong, C. Prakash, S. Debnath, S. Subramaniam, I. Jawahir, S. Dixit, D. Buddhi, A critical review on additive manufacturing of Ti-6Al-4V alloy: microstructure and mechanical properties, J. Mater. Res. Technol. 18 (2022) 4641–4661, https://doi.org/10.1016/j.jmrt.2022.04.055.
[9] M.A. Obeidi, Metal additive manufacturing by laser-powder bed fusion:Guidelines for process optimisation, Results in Engineering 15 (2022) 100473, https://doi.org/10.1016/j.rineng.2022.100473.
[10] M.A. Obeidi, A. Mussatto, M.N. Dogu, S.P. Sreenilayam, E. McCarthy, I.U. Ahad, S. Keaveney, D. Brabazon, Laser surface polishing of Ti-6Al-4V parts manufactured by laser powder bed fusion, Surf. Coat. Technol. 434 (2022) 128179, https://doi.org/10.1016/j.surfcoat.2022.128179.
[11] L.C.B. Carolo, R.E. Cooper O., A review on the influence of process variables on the surface roughness of Ti-6Al-4V by electron beam powder bed fusion, Addit. Manuf. 59 (2022) 103103, https://doi.org/10.1016/j.addma.2022.103103.
[12] F. Huber, T. Papke, C. Kauffmann, R. Rothfelder, P. Krakhmalev, M. Merklein, M. Schmidt, Systematic exploration of the L-PBF processing behavior and resulting properties of β-stabilized Ti-alloys prepared by in-situ alloy formation, Mater. Sci. Eng. A 818 (2021) 141374, https://doi.org/10.1016/j.msea.2021.141374.
[13] K.L. Tan, S.H. Yeo, Surface finishing on IN625 additively manufactured surfaces by combined ultrasonic cavitation and abrasion, Addit. Manuf. 31 (2020) 100938, https://doi.org/10.1016/j.addma.2019.100938.
[14] F. Scherillo, Chemical surface finishing of AlSi10Mg components made by additive manufacturing, Manuf. Lett. 19 (2019) 5–9, https://doi.org/10.1016/j.mfglet.2018.12.002.
[15] S. Bagehorns, T. Mertens, D. Greitemeier, L. Carton, A. Schoberth, Surface finishing of additive manufactured Ti-6Al-4V - a comparison of electrochemical and mechanical treatments, Eucass 2015 (2015).
[16] E. Lyczkowska, P. Szymczyk, B. Dybała, E. Chlebus, Chemical polishing of scaffolds made of Ti-6Al-7Nb alloy by additive manufacturing, Archives of Civil and Mechanical Engineering 14 (2014) 586–594, https://doi.org/10.1016/j.acme.2014.03.001.
[17] P. Tyagi, T. Goulet, C. Riso, R. Stephenson, N. Chuenprateep, J. Schlitzer, C. Benton, F. Garcia-Moreno, Reducing the roughness of internal surface of an additive manufacturing produced 316 steel component by chempolishing and electropolishing, Addit. Manuf. 25 (2019) 32–38, https://doi.org/10.1016/j.addma.2018.11.001.
[18] J.M. Flynn, A. Shokrani, S.T. Newman, V. Dhokia, Hybrid additive and subtractive machine tools - research and industrial developments, Int. J. Mach. Tool Manuf. 101 (2016) 79–101, https://doi.org/10.1016/j.ijmachtools.2015.11.007.
[19] Y. Kaynak, O. Kitay, The effect of post-processing operations on surface characteristics of 316L stainless steel produced by selective laser melting, Addit. Manuf. 26 (2019) 84–93, https://doi.org/10.1016/j.addma.2018.12.021.
[20] B. AlMangour, J.-M. Yang, Improving the surface quality and mechanical properties by shot-peening of 17-4 stainless steel fabricated by additive manufacturing, Mater. Des. 110 (2016) 914–924, https://doi.org/10.1016/j.matdes.2016.08.037.
[21] A.H. Maamoun, M.A. Elbestawi, S.C. Veldhuis, Influence of shot peening on AlSi10Mg parts fabricated by additive manufacturing, J. Manuf Mater. Process. 2 (2018), https://doi.org/10.3390/jmmp2030040.
[22] M.A. Bernevig-Sava, C. Stamate, N.M. Lohan, A.M. Baciu, I. Postolache, C. Baciu, E. R. Baciu, Considerations on the surface roughness of SLM processed metal parts and the effects of subsequent sandblasting, IOP Conf. Ser. Mater. Sci. Eng. 572 (2019), https://doi.org/10.1088/1757-899X/572/1/012071.
[23] A. El Hassanin, M. Troiano, F. Scherillo, A.T. Silvestri, V. Contaldi, R. Solimene, F. Scala, A. Squillace, P. Salatino, Rotation-assisted abrasive fluidised bed machining of alsi10mg parts made through selective laser melting technology, Procedia Manuf. 47 (2020) 1043–1049, https://doi.org/10.1016/j.promfg.2020.04.113.
[24] E. Atzeni, M. Barletta, F. Calignano, L. Iuliano, G. Rubino, V. Tagliaferri, Abrasive fluidized bed (AFB) finishing of AlSi10Mg substrates manufactured by direct metal laser sintering (DMLS), Addit. Manuf. 10 (2016) 15–23, https://doi.org/10.1016/j.addma.2016.01.005.
[25] E. Manco, F. Scherillo, C. Guerrera, M. Bruno, A. El Hassanin, S. Franchitti, R. Borrelli, L. Esposito, Influence of chemical machining on axial fatigue behaviour of electron beam melted Ti6Al4V parts, Manuf. Lett. 35 (2023) 6–10, https://doi.org/10.1016/j.mfglet.2022.11.001.
[26] E. Maleki, S. Bagherifard, M. Bandini, M. Guagliano, Surface post-treatments for metal additive manufacturing: Progress, challenges, and opportunities, Addit. Manuf. 37 (2021) 101619, https://doi.org/10.1016/j.addma.2020.101619.
[27] D. Bourell, J.P. Kruth, M. Leu, G. Levy, D. Rosen, A.M. Beese, A. Clare, Materials for additive manufacturing, CIRP Ann. Manuf. Technol. 66 (2017) 659–681, https://doi.org/10.1016/j.cirp.2017.05.009.
[28] M.A. Obeidi, E. McCarthy, B. O'Connell, I.U. Ahad, D. Brabazon, Laser polishing of additive manufactured 316L stainless steel synthesized by selective laser melting, Materials 12 (2019), https://doi.org/10.3390/ma12060991.
[29] M. Obeidi, E. Mccarthy, S. Ubani, I. Ahad, D. Brabazon, Effect of surface roughness on CO2 laser absorption by 316L stainless steel and aluminum, Mater. Perform. Charact. 8 (2019) 20180091, https://doi.org/10.1520/MPC20180091.
[30] X. Liu, H. Wang, K. Kaufmann, K. Vecchio, Directed energy deposition of pure copper using blue laser, J. Manuf. Process. 85 (2023) 314–322, https://doi.org/10.1016/j.jmapro.2022.11.064.
[31] K. Takenaka, Y. Sato, N. Yoshida, M. Yoshitani, M. Heya, M. Tsukamoto, Additive manufactured of pure copper by blue diode laser induced selective laser melting, J. Laser Appl. 34 (2022) 042041, https://doi.org/10.2351/7.0000748.
[32] M. Ahmed Obeidi, E. McCarthy, D. Brabazon, Methodology of laser processing for precise control of surface micro-topology, Surf. Coat. Technol. 307 (2016) 702–712, https://doi.org/10.1016/j.surfcoat.2016.09.075.
[33] S. Lewin, I. Fleps, J. Åberg, S.J. Ferguson, H. Engqvist, C. Öhman-Mägi, B. Helgason, C. Persson, Additively manufactured mesh-type titanium structures

for cranial implants: E-PBF vs. L-PBF, Mater. Des. 197 (2021), https://doi.org/10.1016/j.matdes.2020.109207.
[34] S. Chowdhury, N. Yadaiah, C. Prakash, S. Ramakrishna, S. Dixit, L.R. Gupta, D. Buddhi, Laser powder bed fusion: a state-of-the-art review of the technology, materials, properties & defects, and numerical modelling, J. Mater. Res. Technol. 20 (2022) 2109–2172, https://doi.org/10.1016/j.jmrt.2022.07.121.
[35] L. Chen, B. Richter, X. Zhang, K.B. Bertsch, D.J. Thoma, F.E. Pfefferkorn, Effect of laser polishing on the microstructure and mechanical properties of stainless steel 316L fabricated by laser powder bed fusion, Mater. Sci. Eng. A 802 (2021) 140579, https://doi.org/10.1016/j.msea.2020.140579.
[36] F. Calignano, Investigation of the accuracy and roughness in the laser powder bed fusion process, Virtual Phys. Prototyp. 13 (2018) 1–8, https://doi.org/10.1080/17452759.2018.1426368.
[37] U. Prisco, A. Astarita, A. El Hassanin, S. Franchitti, Influence of processing parameters on microstructure and roughness of electron beam melted Ti-6Al-4V titanium alloy, Mater. Manuf. Process. 34 (2019) 1753–1760, https://doi.org/10.1080/10426914.2019.1683576.
[38] D. Campanella, G. Buffa, A. El Hassanin, A. Squillace, F. Gagliardi, L. Filice, L. Fratini, Mechanical and microstructural characterization of titanium gr.5 parts produced by different manufacturing routes, Int. J. Adv. Manuf. Technol. 122 (2022) 741–759, https://doi.org/10.1007/s00170-022-09876-9.